IJCS INTERNATIONAL JOURNAL OF CONSERVATION SCIENCE
ISSN: 2067-533X Volume 8, Issue 4, October-December 2017: 565-580 www.ijcs.uaic.ro

SIMULATION OF A PORTUGUESE LIMESTONE MASONRY STRUCTURE SUBMITTED TO FIRE: 3D ULTRASONIC TOMOGRAPHY APPROACH

Edite MARTINHO[1,*], Amélia DIONÍSIO[1], Manuela MENDES[2]

[1] CERENA, Instituto Superior Técnico, Lisbon University, Av. Rovisco Pais, 1049-001, Lisbon, Portugal
[2] ICIST, Instituto Superior Técnico, Lisbon University, Av. Rovisco Pais, 1049-001, Lisbon, Portugal

Abstract

A multianalytical approach combining 3D ultrasonic tomography, FESEM, capillary absorption coefficient, open porosity and elastic constants (σ, E, μ and K) has been applied to characterize the extent and severity of Lioz limestone decay processes induced by fire, as well as the performance of two consolidants (ethyl silicate and nanolime). Samples (15 cm × 3 cm × 3 cm) were partially buried in fine sand (to mimic the real situation of stone blocks in masonry structures) and a section of 15 cm × 3 cm × 0.5 cm was exposed to direct heat (600ºC). The region directly exposed to heat exhibited lower P-wave velocity and more intense fissuration whereas the areas more protected showed thermal etch pits structures. Ethyl silicate showed better performance than nanolime and 3D ultrasonic tomography allowed estimating the depth reached by this consolidant.

Keywords*: Fire decay; Lioz limestone; Consolidation; 3D ultrasonic tomography; FESEM*

Introduction

Fires at artistic buildings and monuments drew attention to the severe damage that fire may cause in their stones and structures. Permanent changes in their mineralogical composition, textural and structural properties can occur [1]. While high temperatures reached during a fire can produce short-term irreversible physical-chemical changes, the ashes and fumes may have a longer-lasting effect [2]. Therefore, a diagnosis of the deterioration decay degree is necessary in order to select the most appropriate conservation technique. Lioz limestone has been used since ancient times in monuments and currently in building facades, not only in Portugal but also abroad. Given its abundant use, especially in historic buildings, some of which affected by fires [3], there is a special interest in evaluating its fire decay and how to conserve and preserve it. Like marbles, that have received particular attention since they are considered a noble material, Lioz limestone also has a very simple mineralogical composition and so, the damage caused by heat may also be associated to calcite's anisotropic thermal expansion. Elevated temperatures lead to expansion of this mineral in the crystalographic c-direction and contraction in perpendicular directions [4] resulting in the formation of microfractures or microcracks [5-8] and also modifications on stone fabric (grain size, grain aspect ratios, grain-shape-preferred orientation and texture). These aspects affect materials behavior both physically and mechanically and thus their durability.

* Corresponding author: edite.martinho@tecnico.ulisboa.pt

As well known, when stone is heated during a fire, a steep temperature gradient is generated from the surface to the inner parts of the stone [9], i.e., the stone surface is subjected to very high temperatures, that drastically decreases inwardly. As a result, the decay is constrained to first few centimeters of stone. Therefore, the current research program intended to assess the impact of high temperature and subsequent consolidation intervention on Portuguese Lioz limestone masonry/panels. Lioz samples were partially buried in fine sand, exposing directly to heat only a single face in order to mimic the real situation of stone blocks in masonry/cladding structures. Although the subject of the effects of temperature on the natural stones have been studied in laboratory by several researchers, using different set ups such as sample dimensions, heating rates, atmospheres, temperatures, etc. [10-16], there are only a few literature works that try to close replicate the real-world conditions, i.e., to reflect the most common exposure of a single stone face to a fire event and subsequently to heat [17]. Additionally the analysis of physical and mechanical stone properties changes has been limited to 1D or 2D information [1, 18-20], although more high-resolution and non-destructive methodologies are required in the assessment and preservation of cultural heritage built in stone. In order to overcome the limitation related to the 1D and 2D assessment of dynamic elastic modulus, this study intended to measure the transit times of longitudinal waves, by non-destructive ultrasonic method, to built a 3D velocity distribution model based on a tomographic inversion [21, 22]. Using the promising 3D elastic velocity models (for reference, heat artificially decayed and consolidated samples), the strength was estimated and compared in order to evaluate fire decay and subsequent consolidation treatment (effectiveness and penetration depth).

Materials and experimental procedure

Stone material

A Portuguese limestone-Lioz was selected on the basis of its widespread use as building material and ornamental stone in contemporaneous building facades not only in Portugal but in works spread all over the world and also in Romanesque, Gothic, Renaissance, Baroque and Neoclassical monuments. Moreover significant and visible structural and aesthetic changes in Lioz appearance have been observed after exposure to high temperatures.

Lioz is a beige colored microcrystalline, bioclastic and calciclastic limestone, with abundant fossils remains (rudists), which give an aesthetics peculiarity to this ornamental stone (Fig. 1a). It is dated Cretaceous in age and formed in an area of shallow sea with warm, clear water that stimulated the proliferation of organisms with calcium carbonate skeletons. Lioz usually presents very low values of properties related to fluid transport in porous media and porosity, and medium to high values of uniaxial compressive and flexural strength [23]. In what concerns thermal linear expansion coefficient, maximum values for Lioz are comprised between 3.3-5.9x10^{-6} per ºC [23], reflecting that of calcite. Further details on Lioz geological context, petrography, mineralogy and physical-mechanical properties can be found in Figueiredo and Aires-Barros [23, 24].

Stone samples used in this experimental research were obtained from quarries in Pêro Pinheiro (Sintra, Portugal) and later cut in laboratory into parallelepiped shape using a diamond saw. The specimen surfaces were finished using carborundum #180 (silicon carbide) without any other surface finish. Three prismatic specimens (15×3×3cm) were used for the laboratory experiments (identified as SP1, SP2 and SP3). In this study the terminology ‘‘reference’’ will be used when mentioning physical–mechanical and microstructural results achieved in unheated limestone specimens.

Fig. 1. Lioz limestone with different surface finishes: (a) Polished and (b) Saw cut.

Laboratorial heating procedure

To simulate the heating generated by fire on natural stone and thus replicate the damage generated, it was used a laboratorial muffle (Ehret, maximum temperature of 1100°C) with an oxidizing environment. The stone samples were partially buried in fine sand (Fig. 2) prior to placing them in the muffle exposing a single face (15×3×0.5cm) to direct heating in order to mimic the real situation of stone blocks in masonry structures. The samples were placed in the muffle at 600°C for 23 h. The warming up started from room temperature (20ºC) and followed a heating gradient of 9.6ºC min^{-1}. After heat exposure, the samples (referred to hereinafter as "heated") were left to return to ambient conditions, removed from the sand and subjected to several evaluations, as mentioned hereafter.

Fig. 2. Sample encased in fine sand.

Consolidation: products and procedure

Two ready to use commercial consolidant products were evaluated: a tetra ethyl-ortho-silicate (TEOS) mixed with white spirit (70% TEOS+ 30% white spirit, Tegovakon®, BIU Internacional), and a dispersion of nanostructured particles of slaked lime in isopropanol

(nanolime), with an average concentration of calcium hydroxide nanoparticles of 1.5 $g \cdot L^{-1}$ (Nanorestore ®, CTS). The SP1 and SP2 samples were treated with nanolime while SP3 sample with TEOS. The consolidation treatment was carried out in stable laboratory conditions (T = 20±2ºC; Hr = 57.5±2.5%) using the direct contact capillarity method, i.e., the liquid being soaked up by the capillary forces of the stone material. The prisms were positioned horizontally on plastic rods, with one lateral face (15.0 × 3.0cm) immersed about 0.5cm in the solution for 24 hours. The consolidation was carried out in one application, with exception of SP1 sample which was subjected to a second application of nanolime. This second application occurred with an interval of 6 weeks between applications with the same procedure. During the consolidation application period, the recipient vessel and samples were encapsulated in a plastic container to prevent evaporation. The amount of product absorbed, expressed as the mass of product per unit surface ($kg \cdot m^{-2}$), was quantified by weighting the samples before and immediately after treatment. All the surfaces in contact with the consolidants were gently cleaned immediately after application with a cloth dampened in the solvent to avoid the formation of superficial deposits. The consolidated specimens were allowed to cure for four weeks after application of the products in stable laboratory conditions in order to promote the formation of amorphous silica (case of consolidant based on silicate) or carbonation of the calcium hydroxide nanoparticles inside stone pores. The dry matter of the consolidants remaining on the treated stones after cure was measured by weighting the samples before treatment and after the curing period (1 month) and expressed as a percentage of the initial weight.

Testing methods/ Evaluation criteria

Several properties evaluations were made before and after heating and after consolidation tests, such as: open porosity, water absorption by capillarity, density and dynamic elastic modulus (determined from ultrasonic velocity method). Moreover, macroscopic (visual appearance) and microscopic features were also evaluated.

An accurate assessment of the heat implications on the porous structure/micro-scale mineralogical and textural changes of the studied stone was conducted by electron microscopy techniques. Stone fragment samples (before and after heat exposure) were examined by field emission scanning electron microscopy (FESEM) with X-ray energy dispersive spectroscopy (EDS). These analyses were carried out with a FESEM Jeol JSM-7001F microscope equipped with an Oxford EDS light elements detector on samples previously sputter coated with a thin gold/palladium film, using an acceleration voltage of 15 kV.

Capillary water absorption and open porosity were measured according to European Standards EN 1925:1999 and EN 1936:2006, respectively [25, 26].

The determination of the wet bulk density involved the measurement of the sample mass (weighted using a Mettler Toledo analytical balance with an accuracy of 0.01 g) and its apparent volume, determined by water displacement method. The samples were immersed in water using a graduated cylinder with accuracy of 2.5 ml.

Mechanical properties were evaluated by dynamic elastic modulus, determined from the ultrasonic velocity method. The P- wave and S-wave travel times were measured, with an accuracy of 0.1μs, using an ultrasonic tester model Steinkamp BP7 with 45 KHz transducers and a Panametrics device model 5800 with 1 MHz transducers, respectively. The P-wave travel time (compressional wave) was measured following a grid with 5.0x5.0mm, with a total of 310 transmitter receiver pairs (Fig. 3). The S-wave travel time (shear wave) was determined at 3 positions of the samples (Fig. 3): near both extremities (C3 and C27) and at the middle section (C14).

A 3D velocity model based on a SIRT tomographic inversion algorithm derived by *M. Mendes* [21] and *J.L. Mari and M. Mendes* [22] was possible to build given the high number of compressional wave transit time measurements. The 3D inversion started, for simplicity, with a constant velocity model. The interactive process stopped when the root-mean-square (RMS)

error reached the accuracy of the measurements (exception for sample SP1, where the accuracy considered after first consolidation treatment was 0.3μs). The initial velocity values were: (i) reference samples v0SP1 = 6500m·s^{-1} (sample SP1), v0SP2 = 8750m·s^{-1} (sample SP2) and v0SP3 = 6500m·s^{-1} (sample SP3); (ii) heated samples v0SP1 = 3750m·s^{-1}, v0SP2=3750m·s^{-1}, and v0SP3 = 3500m·s^{-1}; and (iii) consolidated samples v0SP1 = 3750m·s^{-1} (first and second application), v0SP2 = 3750m·s^{-1} and v0SP3 = 4000m·s^{-1}.

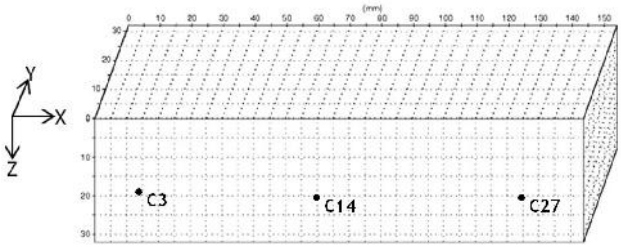

Fig. 3. Layout of measuring of the ultrasonic propagation velocity and position of S-waves measurement points (C3, C14 and C27).

Error analysis

Since only a small number of measurements for each parameter were performed, no statistical analysis of errors was permitted. The error propagation theory was considered in the error estimation.

Results

Figure 4 shows the surface of SP3 sample directly exposed to heat and the opposite face encased in sand, which is representative of what happened to the three samples studied in this laboratory simulation. Visible changes in stone appearance after heat exposure were registered: (i) the exposed side presented a whitish colour with noticeable local loss of stone material (more pronounced near the edges) and this colour modification developed towards the contact zone with sand bed; and (ii) the sides partially buried in sand presented a light grayish color with no significant macroscopically visible decay patterns. A more detailed description of the morphological modifications induced by heat will be described further ahead.

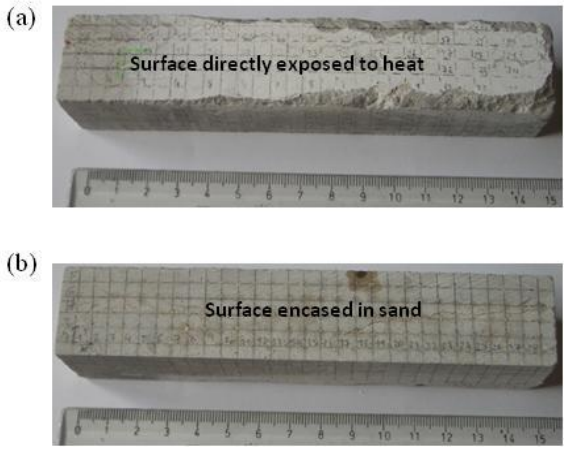

Fig. 4. Comparison of Lioz limestone samples heated to 600ºC: (a) section directly exposed to heat; (b) surfaces encased in fine sand.

The effects of heating and posterior consolidation on open porosity, water absorption coefficient and bulk density are summarized in Table 1. Moreover, a comparison of the water absorption kinetics for SP1 and SP3 samples between reference, heated and consolidated is illustrated in Figure 5.

Table 1. Petrophysical parameters for reference, heated at 600ºC (in fine sand bed) and after consolidation samples.

Parameters	Samples									
	SP1				SP2			SP3		
	Reference	Heated 600^{0}C	1st application consolidant	2nd application consolidant	Reference	Heated 600^{0}C	1st application consolidant	Reference	Heated 600^{0}C	1st application consolidant
Capillary absorption coefficient ($g\,m^{-2}s^{-1/2}$)*	3.851	24.474	26.081	25.092	3.845	31.755	30.091	3.61	30.228	11.337
Open porosity (%)	1.175 (±0.02)	2.720 (±0.02)	2.690 (±0.02)	2.709 (±0.02)	0.546 (±0.02)	2.851 (±0.02)	2.912 (±0.02)	0.941 (±0.02)	2.687 (±0.02)	2.464 (±0.02)
Bulk density (gcm^{-3})	2.723 (±0.06)	2.668 (±0.06)	2.608 (±0.06)	2.611 ((±0.06)	2.678 (±0.06)	2.625 (±0.06)	2.613 (±0.06)	2.713 (±0.06)	2.694 (±0.06)	2.636 (±0.06)

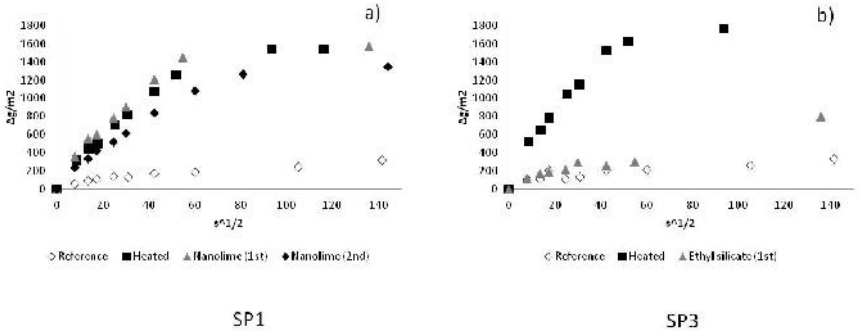

Fig. 5. The effect of temperature and consolidation on capillary water absorption kinetics: (a) sample SP1; (b) sample SP3.

Compressional (VP) and shear (VS) wave velocities, velocity ratio (VP/VS) and elastic parameters (Poisson's ratio, Young's, shear and bulk modulus) for three measured points (C3, C14 and C27) are presented in figure 6. Figures 7, 8 and 9 show the tomograms generated by the 3D inversion of P-wave velocity and also 2D sections (taken at x = 25mm, x = 75mm and x = 125mm) for the three different states of samples.

In the reference samples, the average P-wave velocity were in the range of 5500m·s^{-1} and 7000m·s^{-1} for both samples SP1 and SP3 (Figs 7a, 9a) and for the sample SP2 between 8500m·s^{-1} and 9000m·s^{-1} (Fig. 8a). SP2 reference sample also had the highest values in all the other mechanical parameters (Fig. 6), in agreement with the measured open porosity value (about half of the measured values for samples SP1 and SP3). As shown in figures. 6, 7b, 8b and 9b, the stone samples strength decreased with heating; some elastic parameters (VP, *E*, μ and *K*) revealed a reduction exceeding 40%. The same trend was observed on the tomograms: an average decrease in the VP values of 36%, 56% and 50%, was registered for samples SP1, SP2 and SP3, respectively. The 2D sections showed that the VP velocity was lower near the surface directly exposed to heat (about 3000-3500m·s^{-1}) in comparison to the zones encased by sand (approximately 4000ms^{-1}), reflecting a reduction of the material strength towards the heat surface. The measured petrophysical parameters were in agreement with these results: after heating, open porosity increased 2.3 (sample SP1), 5.2 (sample SP2) and 2.9 (sample SP3) times the initial (reference) values (Table 1). After heating, samples showed significant differences in capillary water absorption. Even though the analysis of capillary water absorption did not involve completely submerging the samples in water, the final quantity of absorbed water was almost eight times the initial values (Fig. 5). The capillary absorption coefficient increased about 6.4 (sample SP1), 8.3 (sample SP2) and 8.4 (sample SP3) times compared to the reference values (Table 1 and Fig. 5).

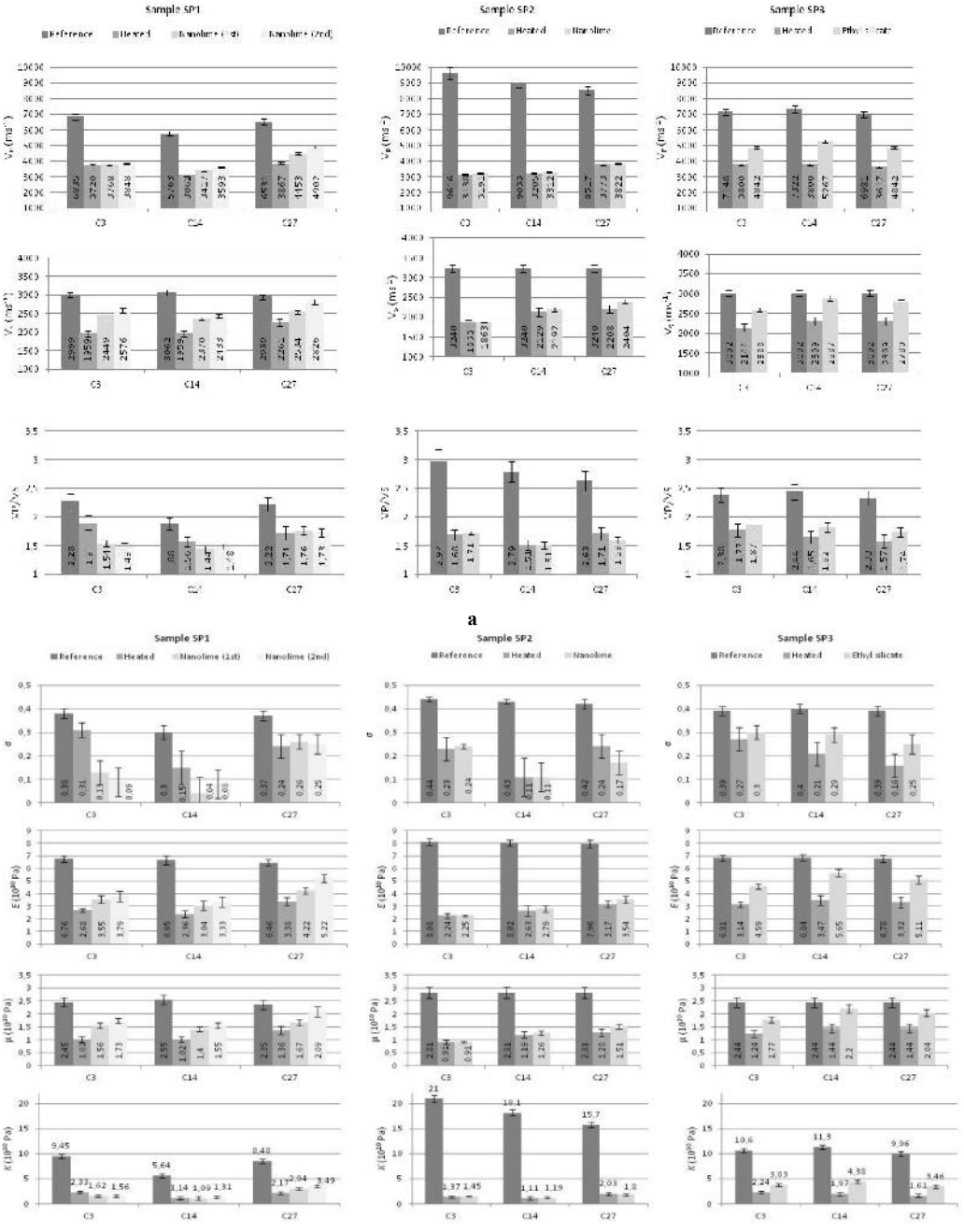

Fig. 6. Elastic parameters for reference, heated 600ºC encased in sand and after consolidation samples: (a) VP, VS and VP/VS; (b) σ, *E*, μ and *K*.

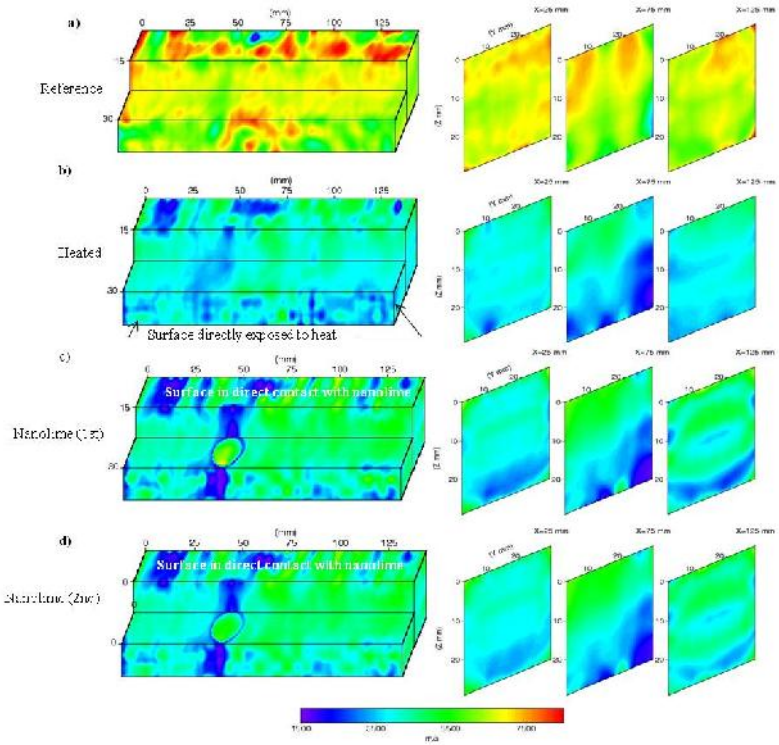

Fig. 7. 3D block and 2D sections (for x=25, 75 and 125 mm) with the P-waves velocity distribution for sample SP1: reference (a); thermally damaged (b); after first application of nanolime (c); after second application of nanolime (d).

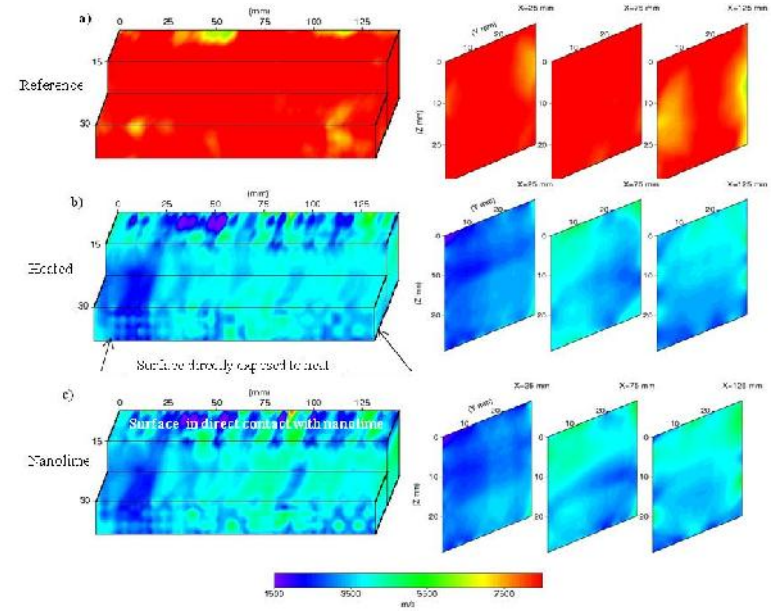

Fig. 8. 3D block and 2D sections (for x=25, 75 and 125 mm) with the P-waves velocity distribution for sample SP2: reference (a); thermally damaged (b); after first application of nanolime (c);

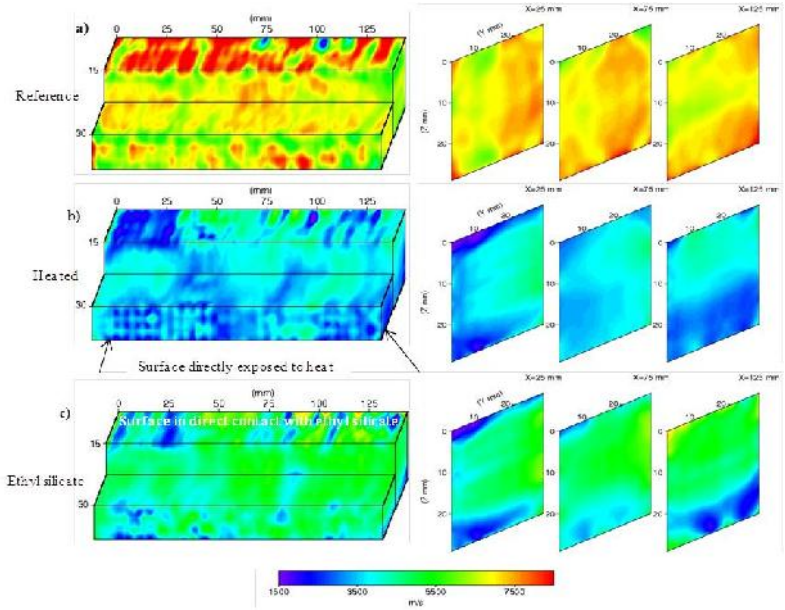

Fig. 9. 3D block and 2D sections (for x=25, 75 and 125 mm) with the P-waves velocity distribution for sample SP3: reference (a); thermally damaged (b); after application of ethyl silicate (c).

Field emission scanning electron microscopy (FESEM) images confirmed that the artificial heat of limestone samples induced changes in porosity structures (Fig. 10), with different intensity and typology depending on the heat exposure or heat protection by the encasing layer of fine sand. Indeed, it was possible to verify a clear microstructural contrast between more exposed areas to heat and those protected by sand (Fig. 10a and b). The strong temperature gradients between the exposed surface and sub-surface areas caused several microstructural modifications. The most exposed areas presented a clear detachment from the remaining material with a thickness of approximately 500µm, and within these areas several microcracks quite open sub-parallel to surface formed (Fig. 10b). In the innermost areas, protected by sand (Fig. 10c, d), these type of fissures were rarer, and with smaller aperture. Nevertheless, these regions still showed some heating effects; besides intergranular porosity, it was developed prominent intragranular porosity within calcite crystals, also called surface thermal micro-etching of calcite crystals (Fig. 10d). These fine pores of <1µm diameter and 0.1-0.21µm depth were not present in this limestone prior to heat (Fig. 10e, f). Indeed, these differences in spatial distribution, interconnection and size of pores cross the section clearly justified the quantity and speed of water absorption by capillary, as registered after heating.

Table 2 presents both amounts of consolidating products consumed and dry matter deposited in Lioz stone specimens.

Table 2. Consolidating products: amount of product consumed and dry matter.

Sample	Consolidant	Amount of product consumed (kgm^{-2})	Dry matter (%)
SP1- 1st application	Nanolime	0.540	0.018
SP1- 2nd application		0.596	0.012
SP2		0.528	0.032
SP3	Ethyl silicate	0.673	0.209

The consolidation treatment with ethyl silicate promoted a higher consumption of product (about a quarter more) and significant higher amount of dry matter deposited. The dry

matter ratios were for SP3:SP1 11.8 and SP3:SP2 17.7, and 6.4 in the 1st and 2nd applications, respectively. The amount of ethyl silicate and nanolime absorbed was about 70% and 6.5%, respectively of the amount of product consumed. As can be seen from Table 1 and Figures 6, 7c and 8c, the first application of nanolime in the SP1 and SP2 samples did not improved significantly the physical and mechanical properties of the samples. Changes in capillary absorption coefficient and open porosity were not significant (the variations are within the error limits) and the average increase in the elastic parameters values was less than 20% and 15% in SP1 and SP2, respectively. Some mechanical parameters (VP/VS and *K*) even showed lower values than those obtained in the heated samples. Nevertheless, these values fall within the error limits (Fig. 6) and thus without physical significance. The same trend was observed for Poisson's ratio (σ), excluding C3 and C14 for sample SP1. Moreover, the improvement in physical and mechanical properties of SP1 sample after the second application of nanolime was very small (Table 1 and Figs 6 and 7d). In most of the parameters the increase was less than 11% and there were also parameters that even registered a decrease (although within the error limits); the greatest increase was observed in the parameters *E*, *K* and μ in C3 point (between 19% and 25%).

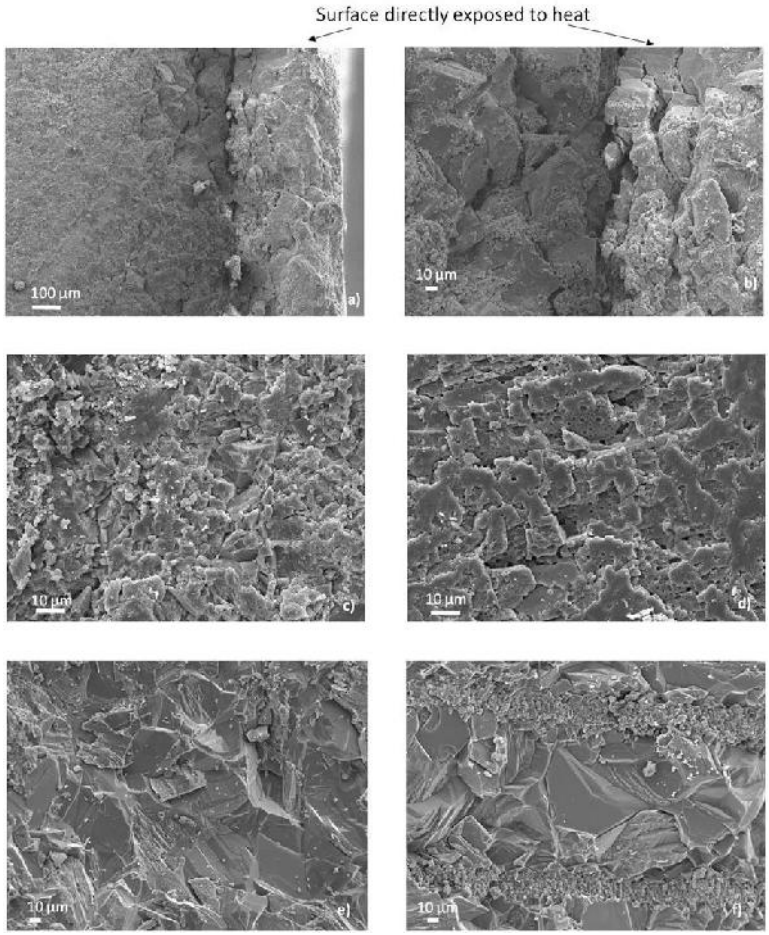

Fig. 10. FESEM images of artificially heated Lioz limestone: (a, b) surface directly exposed to heat exhibiting fissures and detachment; (c, d) surface protected to heat mainly showing development of micro-etching pits inside calcite crystals; FESEM images of reference Lioz limestone: (e, f) calcite crystals without intragranular porosity and low development of intergranular structures.

Regarding the 3D P-wave velocities distribution, there were no significant differences registered between the first and second application of nanolime. The single application of ethyl silicate produced an improvement in physical and mechanical properties of the sample SP3 (Table 1, Figs 6 and 9c). Indeed, this consolidant had a stronger impact on the water absorption kinetics reduction (Fig. 5) although it was not so marked in terms of open porosity reduction (Table 1). Concerning the heated sample, the increase in the P-and S-wave velocities was, on average, higher than 20% while the parameters σ, *E*, μ and *K* showed an increase of more than 30%; VP / VS was the parameter that recorded the smallest increase (about 8%). The capillary water absorption coefficient and open porosity modifications reflected the observed improvement in mechanical properties (3.5 and 1.1 times the values of the heated sample for capillary water absorption and open porosity, respectively).

Changes in bulk density caused by thermal shock and consolidation treatment were very small and in some cases they are even within the error limits (Table 1).

Discussion

The tomograms with the 3D distribution of P-wave velocities clearly indicate that Lioz is a heterogeneous stone (Figs 7a, 8a and 9a). The SP1 and SP3 samples had similar distribution of velocities (5500 – 7500m·s^{-1}); SP2 showed higher velocities (about 8500m·s^{-1}) with a more homogeneous distribution. Despite the Lioz heterogeneity, the physical and mechanical properties of the three samples after heating were similar, showing, contrary to expectations, a stronger decay in SP2 sample. As can be seen from Table 1, reference Lioz presents low porosity and water absorption capacity, analogous to what happens in marbles. In stones with similar properties, the physical breakdown caused by heating is due to the micro-cracking generated by the thermal expansion of minerals [9, 27], in this case, of the calcite [28, 29]. New fissures were developed by the thermal expansion of individual grains of calcite. Indeed FESEM images showed that the most affected areas were those closer to the heat source. Calcite has a highly anisotropic thermal expansion coefficient α, i.e. extreme expansion parallel and contraction normal to the crystallographic c-axis [8, 30]. The absence of a more porous matrix, which could absorb the stresses caused by the thermal expansion of the calcite grains, increases the possibility of mechanical breakdown of Lioz limestone as shown by the results (Table 1, Figs. 6, 7b, 8b, 9b and Fig. 10a and b). As it has already been reported in building stones with low porosity, changes in porosity, caused by fire, can reach thirteen times the initial value [31]; independently of stone type, the lower the initial porosity the greater the porosity increase generated during fire [9]. High porosity values determine the existence of more inter-granular space that could bear the thermal expansion of grains and, therefore, the changes of the overall values of porosity are slighter than in compact materials [27]. In the current study, changes between 2.3 and 5.2 times the initial porosity (Table 1) were registered. These values fall short of that mentioned by *M. Gomez-Heras et al.* [27], probably, due to the protection of the Lioz by the sand bed during the heating. However, the sample with a lower initial porosity (SP2) recorded the highest increase of the porosity (5.2 times the initial value) after heating confirming what has been observed by several other authors. This may be the cause of the strong decay observed in this sample: on average, a reduction of 59% of the elastic parameters was observed against 45% and 47% in SP1 and SP3 samples, respectively (Figs. 6, 7b, 8b and 9b). Although SP2 reference sample showed the lowest porosity, the capillary absorption coefficient is similar to the other samples. This may be related to the type of voids (geometry and connection); since porosity is lower, probably, the voids are narrower (mainly micro fissures) and therefore, the water uptake occurs more quickly. After heating, the three samples have identical porous volumes and similar porosity structures which may explain the fact that the capillary absorption coefficient nor the open porosity differ significantly in the three

samples (Fig. 5). As a consequence of the increase porosity and capillary absorption coefficient, the heated samples exhibit lower values of elastic parameters; the increase in pore amount and size is responsible for significant decreases in mechanical properties of weathered stones [20]. As noted above, the reduction in the elastic parameter values, due to heating, seems to be related to the initial porosity of the stone; this reduction is lower in the sample which has higher porosity (SP1). In this stone type (carbonated and very low porosity), the initial porosity controls the rate of decay caused by heating. Despite the protection of the sand bed, an average degradation of about 50% in those properties was recorded. At mesoscale, the samples surface in direct contact with the furnace atmosphere is the most damaged by heat (Fig. 4). This is in agreement with the results of tomography. In the 2D sections of P-waves velocities distribution (Figs. 7b, 8b and 9b), a decrease of the velocity in depth is visible, i.e., in the area protected by the sand bed, the velocity is greater than in the area directly exposed to the heat. FESEM images corroborate the previous results: the areas with higher density of fissures are those that were near to the heat source without any protection. The most protected parts of the samples (involved by the fine sand) were also thermally affected but the type and extent of damage was distinct. In these last areas the porosity structures were mainly composed of intragranular micro-etching features (Fig. 10c and d).

Similarly, to what happens in weathered stones subjected to different environmental conditions (changes in temperature and humidity, presence of salts, etc.), the improvement of physical and mechanical properties of weathered stones by fire can also be done by applying consolidation treatments. The effectiveness of the consolidation is known to be influenced by a plurality of parameters such as, stone type and properties, characteristics of the consolidant (in terms of active principle, solvent and the concentration of the components), application procedure, amount of applied product and environmental conditions [32]. In the current research, regarding the mentioned parameters were only different the consolidant characteristics. So, the improvement in physical and mechanical properties of the sample treated with ethyl silicate (SP3) relatively to samples treated with nanolime (SP1 and SP2) is mainly related to the consolidants characteristics. This fact was also proven through the analysis of the dry mass deposited in stone after curing time. Indeed, values of dry mass 10 times higher were reached when ethyl silicate was applied (Table 2). This product penetrates easily in the porous materials; it is absorbed by the stone, hydrolyzed by water to form silanols that then polymerize in a condensation reaction and form a polymer that produces the strength increase [32]. Regarding 2D sections of P-waves velocities distribution, a homogenous distribution of velocity with values of approximately 5500m·s^{-1} can be observed up to 20mm depth (Fig. 9c). So, the penetration depth of the consolidant can be estimated at 2 centimeters. Penetration depth is considered as a key parameter to evaluate the efficacy of a treatment, since an insufficient penetration could lead to treatment failure due to the inability of reaching the unweathered substrate and, therefore, the creation of a discontinuity between the impregnated layer and the underlying one [33]. Nevertheless, the elastic modulus (E) increased, but above the level of the unweathered stone (Table 1) and thus the risk of delamination by over strengthening the surface layer is minimized. The significant reduction of water absorption by capillarity registered in sample SP3 after consolidation can be explained by the fact that ethyl silicate consolidants are known to make the treated stone hydrophobic for several weeks after treatment [34]. The mechanical characteristics of the SP2 sample are worse than those of SP1 sample after the first application of nanolime (Figs. 6, 7c and 8c). The samples properties remained practically unchanged after consolidation. Based on the P-waves velocities distribution tomograms (Figs. 8b and c) it is possible to infer that the lower velocity zones remained almost unchanged after consolidation, as the case of the area of low velocity clearly visible in 2D section x = 25mm. In the SP1 sample, the first consolidation caused a slight improvement in the stone properties (Figs 6 and 7c). Similarly, to that observed in the SP3 sample, VP values are lower as the depth increases (Fig. 7c), showing that the nanolime did not reached the opposite face. The

distribution of velocity values allowed to deduce that nanolime has a heterogeneous distribution within the stone substrata (unlike observed in SP3 sample) and it is not possible to clearly establish the depth achieved. The second application of nanolime, also did not produced visible improvement in the P-waves velocity distribution (Fig. 7c and d), although there has been registered absorption of this consolidant and a slight reduction of water absorption capability of the stone material. Indeed and according to *P. D'Armada and E. Hirst* [35], the treatment with nanolime has little influence on water transport properties (capillary suction) of the treated materials. Nevertheless, a slight improvement was registered in the other elastic parameters (Fig. 6). The current results are opposite to what happened to the study performed by *Z. Slížková and D. Frankeová* [36] when an improvement in the physical and mechanical characteristics of a limestone (not affected by heat) was observed after multiple application of a nanolime product. Nanolime does not seem to be the most suitable consolidant for this case, i.e., for limestone exposed to high temperature, since this consolidation product does not have a significant penetration capability required to guarantee a mass consolidation effect. One reason could be the low porosity of the Lioz stone even after heated (between 2.7 and 2.9%). According to *A.P. Ferreira and J. Delgado Rodrigues* [32], in general, the amount of product absorbed by the carbonate stones depends strongly of the stone porosity. Their results showed that is extremely difficult to treat carbonate stones with porosity lower than around 18%. The poor performance of nanolime may also be related to the low number (only two) of applications. Indeed, the commercial product used can be considered of low concentration, with an average concentration of CaOH nanoparticles of $1.5 g \cdot L^{-1}$. P. *D'Armada and E. Hirst* [35] verified that the compressive, flexural and surface cohesion strengths of carbonate materials treated with nanolime increased with the number of applications. Moreover, these authors concluded that the solvent used clearly influence their results: nanolime in ethanol seemed to be a more effective than in isopropanol (used in the current laboratorial study). Furthermore, *D. Costa and J.D. Rodrigues* [37] concluded that nanolime has low capability to impregnate high porous carbonate materials (such as Ançã limestone) and thus almost no consolidation effect was detected, similarly to what happened in the present case. Nevertheless, ethyl silicate produces significant improvements in spite of the low porosity after heating (2.7%) and the application procedure. Moreover, ethyl silicate in general is known to be less efficient on carbonate stones than on silicate ones [34].

The tomograms of the sample SP1 (Fig. 7) showed a low velocity zone (located at x = 50mm; y = 15-30 mm; z = 0-30 mm) more pronounced after both consolidations and not associated with any visible anomaly on the stone surface. This result can be a consequence of local poor reading travel time data.

Conclusions

This study intended to assess the Lioz limestone decay induced by fire when applied in buildings. For this purpose, the protection provided by the stone blocks in masonry/cladding structures was simulated in laboratory through the use of fine sand bedding. It was also evaluated the performance of subsequent consolidation intervention with two commercial products (nanolime and ethyl silicate). The Lioz heating decay was more pronounced in the surfaces directly exposed to high temperatures than in the areas protected by sand. 3D ultrasonic tomography models and FESEM observations performed on the reference and heated samples revealed an interface between the protected and directly exposed to heat surfaces. In general, the 2D P-waves velocities sections showed higher values in the protected surfaces by sand. A significant increase in temperature induced significant changes in porosity structures of Lioz highlighted by FESEM: (i) the most exposed surface and nearby material, exhibited intense fissuration with a clear individualization from the material partially buried in sand; (ii)

the former material also showed signs of thermal decay mainly enhanced by the etch pits structures.

The previous features were also evidenced in terms of significant increase in porosity, capillary water uptake and reduction of density and elastic parameters (the average values reduction was about 50%).

The knowledge of consolidation effectiveness (and durability) of thermally decayed stone materials and of the phenomena involved is still sparse. Therefore, preliminary results regarding the initial performance of two consolidants, an ethyl silicate and a nanolime based product, were also presented. Ethyl silicate seemed to be more suitable to restore some stone cohesion, to seal micro-cracks and thus increase its mechanical strength. Through ultrasound measurements it was possible to estimate that ethyl silicate penetrated to an average depth of 20mm whereas almost insignificant changes in elastic parameters were registered after the second application of nanolime. The low porosity of the Lioz stone, even after heating, and the low capacity of nanolime to impregnate even highly porous materials appear to be responsible for the poor performance of nanolime.

Increase knowledge of the exposure to a sudden increase in temperature, as that occurring during a fire, with stone materials and its interaction with consolidant products provides valuable insight and is thought to be essential for their conservation and mainly preservation.

Acknowledgments

The authors gratefully acknowledge the support of the CERENA (strategic project FCT UID/ECI/04028/2013) and Ceris-ICIST (strategic project FCT UID/ECI/04625/2013).

References

[1] K. Beck, S. Janvier-Badosa, X. Brunetaud, Á. Török, M. Al-Mukhtar, *Non-destructive diagnosis by colorimetry of building stone subjected to high temperatures*, **European Journal of Environmental Civil Engineering, 20**(6), 2016, pp. 643-655.

[2] P. Vazquez, M. Acuña, D. Benavente, S. Gibeaux, I. Navarro, M. Gomez-Heras, *Evolution of surface properties of ornamental granitoids exposed to high temperatures*, **Construction and Building Materials, 104,** 2016, pp. 263–275.

[3] J.F. Canas, *A Igreja de São Domingos de Lisboa*, **Monumentos, 6**, 1997, pp. 68-71.

[4] D.W. Kessler, **Physical and chemical tests on the commercial marbles of the United States**, Technology Papers of the Bureau of Standards, Washington, Government Printing Office, 1919, p. 123.

[5] M. Franzini, C. Gratziu, M. Spampinato, *Degradazione del marmo per effectto di variazioni di temperatura*, **Rendiconti Società Italiana di Mineralogia e Petrologia, 39**(1), 1984, pp. 47-58.

[6] U. Zezza, E. Previde Massara, V. Massa, D. Venchiarutti, *Effect of temperature on intergranular decohesion of the marbles*, **Proceedings of the Vth International Congress on Deterioration and Conservation of Stone**, Lausanne, Switzerland, 1985, pp. 131-140.

[7] S. Battaglia, M. Franzini, F. Mango, *High sensivity apparatus for measuring linear thermal expansion: preliminary results on the response of marbles*, **I1 Nuovo Cimento, 16**,1993, pp. 453-461.

[8] S. Siegesmund, K. Ullemeyer, T. Weiss, E.K. Tschegg, *Physical weathering of marbles caused by anisotropic thermal expansion*, **International Journal of Earth Sciences, 89**(1), 2000, pp. 170-82.

[9] M. Gomez-Heras, S. McCabe, B.J. Smith, R. Fort, *Impacts of Fire on Stone-Built Heritage An Overview*, **Journal of Architectural Conservation, 15** (2), 2009, pp. 47-58.

[10] M. Hajpál, *Behavior of sandstones of historical monuments under thermal influence*, **Periodica Polytechnica, 43(2)**, 1999, pp. 207-218.
[11] M. Hajpál, A. Török, *Mineralogical and colour changes of quartz sandstones by heat*, **Environmental Geology, 46**(3-4), 2004, pp. 311-322.
[12] A. Török, M. Hajpál, *Effect of temperature changes on the mineralogy and physical properties of sandstones. A laboratory study*, **International Journal for Restoration of Buildings and Monuments, 11**(4), 2005, pp. 211-218.
[13] M. Gómez-Heras, R. Fort, M. Morcillo, C. Molpeceres, J.L. Ocaña, *Calentamiento por láser: una técnica mínimamente invasiva para el estudio del calentamiento producido por el fuego en materiales pétreos de construcción*, **Materiales de Construccion, 58**, 2008, pp. 289-290.
[14] A.S. Goudie, R.J. Allison, S.J. McLaren, *The relations between modulus of elasticity and temperature in the context of the experimental simulation of rock weathering by fire*, **Earth Surface Processes and Landforms, 17**(6), 1992, pp. 605-615.
[15] R.J. Allison, A.S. Goudie, *The effect of fire on rock weathering: an experimental study*, **Rock weathering and landform evolution** (Edited by D.A. Robinson and R.B.G. Robinson), John Wiley & Sons, Brighton, England, 1994, pp. 41-56.
[16] A. Ehling, W. Köhler, *Fire damaged natural building stones*, **Applied Mineralogy in Research Economy, Technology, Ecology and Culture (ICAM2000)** (Edited by D. Rammlnair, J. Mederer, T. Oberthur, R.B. Heimann and J. Pentinghaus), A.A. Balkema, Leiden, Netherlands, 2000, pp. 975-978.
[17] R.J. Allison, G.E. Bristow, *The effects of fire on rock weathering: some further considerations of laboratory experimental simulation*, **Earth Surface Processes and Landforms, 24**(8), 1999, pp. 707-713.
[18] J. Rodríguez-Gordillo, M.P. Sáez-Pérez, *Effects of thermal changes on Macael marble: Experimental study*, **Construction and Building Materials, 20**(6), 2006, pp. 355-365.
[19] S. Chaki, M. Takarli, W.P. Agbodjan, *Influence of thermal damage on physical properties of a granite rock: Porosity, permeability and ultrasonic wave evolutions*, **Construction and Building Materials, 22**(7),, 2008, pp. 1456-1461.
[20] E. Franzoni, E. Sassoni, G.W. Scherer, S. Naidu, *Artificial weathering of stone by heating*, **Journal of Cultural Heritage, 14**(3S), 2013, pp. e85-e93.
[21] M. Mendes, *A hybrid fast algorithm for first arrivals tomography*, **Geophysical Prospect, 57**(5), 2009, pp. 803-809.
[22] J.L. Mari, M. Mendes, *High resolution 3D near surface imaging of fracture corridors and cavities by combining Plus-Minus method and refraction tomography*, **Near Surface Geophysics, 10**(3), 2012, pp. 185–195.
[23] A.C. Moura, J.F. Ramos, **Introducao. Rochas Ornamentals,** available online at http://rop.lneg.pt/rop/images/intro/it6.html, [accessed on 27/07/2016].
[24] P. Figueiredo, L. Aires-Barros, *The Lioz: the natural stone of Lisbon*, **Proceedings of the II Congreso Internazionale de la Piedra**, Madrid, Spania, 1998.
[25] * * *, European Committee for Standardization, *Natural stone test methods – determination of water absorption coefficient by capillarity*, **EN 1925,** Brussels, 1999.
[26] * * *, European Committee for Standardization, Natural stone test methods – determination of real density and apparent density, and of total and open porosity, **EN 1936,** Brussels, 2006.
[27] M. Gomez-Heras, *Procesos y formas de deterioro termico en piedra natural del patrimonio arquitectonico*, **PhD Thesis**, Universidad Complutense de Madrid, Faculta de Ciencias Geologicas, 2005.
[28] J.M. Logan, *Laboratory and case studies of thermal cycling and stored strain on the stability of selected marbles*, **Environmental Geology, 46**(3-4), 2004, pp.456-467.

[29] K. Malaga-Starzec, U. Akesson, J.E. Lindqvist, B. Schouenborg, *Microscopic and macroscopic characterization of the porosity of marble as a function of temperature and impregnation*, **Construction and Building Materials, 20**(10), 2006, pp. 939-947.
[30] B.J. Skinner, *Thermal expansion*, **Handbook of Physical Constants**, **Geological Society of America, Memoirs 97** (Edited by S.P. Clark), 1996, pp. 75-96.
[31] M. Gómez-Heras, M. Álvarez de Buergo, R. Fort, M. Hajpál, A. Török, M.J. Varas, *Evolution of porosity in Hungarian building stones after simulated burning*, **Heritage, Weathering and Conservation, 1** (Edited by R. Fort, M. Alvarez de Buergo, M. Gomez-Heras and C. Vazquez-Calvo), Taylor & Francis, 2006, pp. 513-519.
[32] A.P. Ferreira Pinto, J. Delgado Rodrigues, *Stone consolidation: The role of treatment procedures*, **Journal of Cultural Heritage, 9**(1), 2008, pp. 38-53.
[33] G. Amoroso, V. Fassina, **Stone Decay and Conservation: Atmospheric Pollution, Cleaning, Consolidation and Protection,** Elsevier, New York, 1983.
[34] G.W. Scherer, G.S.Wheeler, *Silicate consolidants for stone*, **Key Engineering Materials**, **391**, 2009, pp.1–23.
[35] P. D'Armada, E. Hirst, *Nano-Lime for Consolidation of Plaster and Stone*, **Journal of Architectural Conservation, 18**(1), 2012, pp. 63-80.
[36] Z. Slížková, D. Frankeová, *Consolidation of porous limestone with nanolime: Laboratory study*, **Proceedings of the 12th International Congress on Deterioration and Conservation of Stone**, 21-25 October 2012, New York , USA, 2012, pp. 1-11.
[37] D. Costa, J.D. Rodrigues, *Consolidation of a porous limestone with nanolime*, **Proceedings of the 12th International Congress on Deterioration and Conservation of Stone**, 21-25 October 2012, New York , USA, 2012.

Received: December 13, 2016
Accepted: November 25, 2017